Model-Independent Determination of H_0 and $\Omega_{K,0}$ using Time-Delay Galaxy Lenses and Gamma-Ray Bursts

Shen-Shi Du, 1,5 ★ Jun-Jie Wei, 2,3 Zhi-Qiang You, 4,5 Zu-Cheng Chen, 4,5 Zong-Hong Zhu, 1 † En-Wei Liang 6

- ¹School of Physics and Technology, Wuhan University, Wuhan, Hubei 430072, China
- ²Purple Mountain Observatory, Chinese Academy of Sciences, Nanjing 210023, China
- ³ School of Astronomy and Space Sciences, University of Science and Technology of China, Hefei 230026, China
- ⁴Department of Astronomy, Beijing Normal University, Beijing 100875, China
- ⁵Advanced Institute of Natural Sciences, Beijing Normal University, Zhuhai 519087, China
- ⁶Guangxi Key Laboratory for Relativistic Astrophysics, School of Physical Science and Technology, Guangxi University, Nanning 530004, China

Accepted XXX. Received YYY; in original form ZZZ

ABSTRACT

Combining the 'time-delay distance' ($D_{\Delta t}$) measurements from galaxy lenses and other distance indicators provides model-independent determinations of the Hubble constant (H_0) and spatial curvature ($\Omega_{K,0}$), only based on the validity of the Friedmann-Lemaître-Robertson-Walker (FLRW) metric and geometrical optics. To take the full merit of combining $D_{\Delta t}$ measurements in constraining H_0 , we use gamma-ray burst (GRB) distances to extend the redshift coverage of lensing systems much higher than that of Type Ia Supernovae (SNe Ia) and even higher than quasars, whilst the general cosmography with a curvature component is implemented for the GRB distance parametrizations. Combining Lensing+GRB yields $H_0 = 71.5^{+4.4}_{-3.0}$ km s⁻¹Mpc⁻¹ and $\Omega_{K,0} = -0.07^{+0.13}_{-0.06}$ (1σ). A flat-universe prior gives slightly an improved $H_0 = 70.9^{+4.2}_{-2.9}$ km s⁻¹Mpc⁻¹. When combining Lensing+GRB+SN Ia, the error bar ΔH_0 falls by 25%, whereas $\Omega_{K,0}$ is not improved due to the degeneracy between SN Ia absolute magnitude, M_B , and H_0 along with the mismatch between the SN Ia and GRB Hubble diagrams at $z \gtrsim 1.4$. Future increment of GRB observations can help to moderately eliminate the $M_B - H_0$ degeneracy in SN Ia distances and ameliorate the restrictions on cosmographic parameters along with $\Omega_{K,0}$ when combining Lensing+SN Ia+GRB. We conclude that there is no evidence of significant deviation from a (an) flat (accelerating) universe and H_0 is currently determined at 3% precision. The measurements show great potential to arbitrate the H_0 tension between the local distance ladder and cosmic microwave background measurements and provide a relevant consistency test of the FLRW metric.

Key words: gravitational lensing: strong – gamma-ray burst: general – cosmological parameters

1 INTRODUCTION

The precise value of Hubble constant (H_0) has emerged as one of the most vital cracks in modern cosmology, with beyond 5σ tension between the local (late-universe) determination from Cepheid variable-calibrated Type Ia supernovae (SNe Ia; Riess et al. 2019, 2021) and the high-redshift (early-universe) measurement by Planck cosmic microwave background (CMB; Planck Collaboration et al. 2020) observations based on the Λ Cold Dark Matter (Λ CDM) cosmological model. This issue has spurred intense debate of beyond-ΛCDM dark energy component or early-universe new physics as well as unaccounted-for systematic effects in either or both of the measurements (e.g., Riess et al. 2011; Marra et al. 2013; Verde et al. 2013; Riess et al. 2016; Bernal et al. 2016; Riess 2019; Verde et al. 2019; Freedman et al. 2019; D'Amico et al. 2021; Di Valentino et al. 2021). Meanwhile, various recent measurements of present-day spatial curvature $(\Omega_{K,0})$ have been shown to mutually disagree with each other, leading to another potential cosmic crisis (Di Valentino et al. 2020). New, independent measurements of the H_0 and $\Omega_{K,0}$ are pursued to provide relevant clues to such discrepancies (see Di Valentino et al. 2021 for a recent review).

Time delay cosmography has become a mature field with the combined strengths of modern monitoring and lens modeling of quasar strong gravitational lensing, which provides a novel measurement of H_0 using the time delays between multiple gravitationally- and geometrically-induced images (Refsdal 1964; Blandford & Narayan 1992; Treu & Marshall 2016; Bonvin et al. 2017; Suyu et al. 2018; Oguri 2019; Wong et al. 2020; Birrer et al. 2020; Denzel et al. 2021). The statistical combination of six measurements on different quasar time-delay lenses had reached a 2.4% measurement of $H_0 = 73.3^{+1.7}_{-1.8} \text{ km s}^{-1}\text{Mpc}^{-1}$ in the flat ΛCDM model (Wong et al. 2020); Considering the mass-sheet transformations, which leave the lensing observables unchanged, as the dominant source of residual uncertainty in H_0 estimation, Birrer et al. (2020) obtained $74.5^{+5.6}_{-6.1}$ km s⁻¹Mpc⁻¹ inferring from the TDCOSMO sample with seven lenses. The measurements are not only independent of the early- and late-universe estimates, but are also proposed to control the systematic errors - around 40 strong lensing systems can measure H_0 at a sub-percent level (Jee et al. 2016; Shajib et al. 2019), thus raising the prospect of adjudicating the tension between CMB

^{*} duss.physics@gmail.com

[†] zhuzh@whu.edu.cn

and the local distance ladder. Nevertheless, time-delay cosmography relies on the assumption of a specific background cosmology, and the inferred value of H_0 could be significantly different with using different cosmological models (see Table 6 in Wong et al. 2020). Thus, this measurement is strongly model-dependent.

A more intriguing application of time-delay galaxy lenses (TDGLs) is combining the TDGLs and such reliable distance indicators from other probes to constrain both the H_0 and $\Omega_{K,0}$ via the distance sum rule (DSR; Collett et al. 2019), merely assuming that the light propagates along null geodesics in the Friedmann-Lemaître-Robertson-Walker (FLRW) metric. This method only relies on the validity of the classical FLRW metric and geometrical optics, and infers H_0 and $\Omega_{K,0}$ with TDGLs providing the "time-delay distance" $(D_{\Lambda t})$ and with the distance indicators extending the redshifts to the lens and source to cover that of the lensing systems well. Additionally, the measurement of $\Omega_{K,0}$ from two or more lens-source pairs provides a consistency test of the FLRW metric (Räsänen et al. 2015). Such measurements has been implemented in combinations with, for instance SNe Ia (Collett et al. 2019), multi-messenger gravitationalwave "standard sirens" (Liao 2019), and ultra-compact structure in radio sources (Qi et al. 2020). We also notice that Wei & Melia (2020) proposed using quasars (QSOs) as distance indicators up to $z \sim 5$ to match the distances of lensing systems that can be detectable by the upcoming Rubin Observatory Legacy Survey of Space and Time (LSST; Oguri & Marshall 2010; Ivezić et al. 2019), which is expected to take full advantage of the lensing catalog in hand. While recent works were indicative of the $\sim 4\sigma$ tension between the quasars and flat Λ CDM at high redshifts (e.g., $z \ge 1.5$) and showed the vigilance of using quasars as standardizable candles to constrain cosmological parameters (e.g., Risaliti & Lusso 2019; Lusso et al. 2020; Yang et al. 2020; Velten & Gomes 2020; Khadka & Ratra 2021). This prompts us to further explore robust high-redshift distance indicators to consolidate the independent measurements of H_0 and $\Omega_{K,0}$ in conjunction with TDGLs via the DSR.

Gamma-ray bursts (GRBs) are the most luminous astrophysical phenomenon, which are expected to be emerged as early as death of the first-generation stars ($z \sim 20$). The central engine and radiation mechanisms as well as the jet composition of GRBs, which are responsible for the energetic γ -ray emission, remain inconclusive. Some aspects of the progenitor models have been well investigated in light of the fact that several long-duration GRBs (LGRBs) are observed in association with core-collapse supernova explosions (see e.g., Zhang 2018). Despite these difficulties, the high luminosity of GRBs and the immunity of γ -rays from dust extinctions contribute to their high detectabilities at distances that are far beyond that SNe Ia (or even quasars) are available, thus GRBs are promising objects serving as cosmological probes to provide meaningful cosmological constraints over a wide redshift range (Dai et al. 2004; Liang & Zhang 2005; Ghirlanda et al. 2006; Amati et al. 2008, 2019; Wang et al. 2015; Demianski et al. 2017, 2021; Khadka et al. 2021). One of the most important observational properties of LGRBs is the phenomenological relations between the observed spectral and intensity quantities (radiated γ -ray energy or luminosity) during the prompt phase, among which the Amati correlation (Amati et al. 2002) between the νF_{ν} spectral peak energy, $E_{\rm p}$, and the bolometric isotropic-equivalent radiated energy, E_{iso} , has been extensively explored as the distance indicators of LGRBs (e.g., Amati et al. 2008, 2019; Demianski et al. 2017, 2021). The main obstacles that preclude the cosmological use of GRBs come from the potential selection effects, the "circularity problem" in calibrating the GRB luminosity correlations, and their possible redshift evolutionary effects (see a recent review by Wang et al. 2015). Several works have investigated the observational selection effects and show a general conclusion that such effects, even though still debated, might be minor (e.g., Amati 2006; Butler et al. 2009; Nava et al. 2012; Demianski et al. 2017). The circularity has been effectively overcome with several reliable calibration procedures (Wang et al. 2015; Amati et al. 2019). We will elaborate on the impact of possible redshift evolutionary effects on the Amati correlation when modelling the GRB distance indicators.

In this work, we propose to combine the $D_{\Lambda t}$ measurements from TDGLs and distances determined with the GRB Hubble diagram to restrict H_0 and $\Omega_{K,0}$ via the DSR. The general cosmography with an arbitrary spatial curvature component is implemented for the GRB distance parametrizations, with which the bounds of H_0 and $\Omega_{K,0}$ are contributed by both the GRB distances and $D_{\Delta t}$. To alleviate the circularity, we simultaneously fit the GRB distance indicators and the parameters in theoretical distances in an effective Bayesian framework, and H_0 and $\Omega_{K,0}$ can be obtained by marginalizing over the remaining parameters. The rest of this paper is arranged as follows. In Section 2, we depict our method to determine the H_0 and $\Omega_{K,0}$ with the combined observations of TDGLs and the popular high-redshift probes, including the most recently released SNe Ia, GRBs, and QSOs, which we denote as standardizable-candle (SC) objects hereafter. The observational data and likelihood constructions are detailed in Section 3. We present the results and discussions in Section 4. Summary is made in Section 5.

2 METHODOLOGY

2.1 Constraining Hubble constant and spatial curvature through distance sum rule

In what follows, we present the method for simultaneously estimating the H_0 and $\Omega_{K,0}$ with only the homogeneity and isotropy ansatz in cosmology, stating that the space-time is described by the FLRW metric.

$$ds^{2} = -c^{2}t^{2} + a^{2}(t) \left[\frac{dr^{2}}{1 - \kappa r^{2}} + r^{2}d\Omega^{2} \right], \tag{1}$$

where c is the speed of light, $a(t)=(1+z)^{-1}$ is the scale factor, and the dimensionless curvature $\kappa=1,0$, and -1 corresponds to a spatially closed, flat, and open universe, respectively. The cosmic expansion rate is defined as $H(z)\equiv \dot{a}(t)/a(t)$ with its present value is H_0 (hereafter, the subscript "0" represents the present value), which acts as a normalization of the Hubble diagram. Let $D_{\rm A}(z_s,z_l)$ be the angular diameter distance of a source emerging at redshift z_s as lensed at z_l , where subscripts "s" and "l" correspond to source and lens, respectively. Assuming that the geometrical optics holds, the dimensionless co-moving distance, $d(z_s,z_l)\equiv (1+z_s)H_0D_{\rm A}(z_s,z_l)/c$, is given by

$$d(z_{\mathcal{S}}, z_{\mathcal{I}}) = \frac{1}{\sqrt{|\Omega_{K,0}|}} \sin \left(\sqrt{|\Omega_{K,0}|} \int_{z_{\mathcal{I}}}^{z_{\mathcal{S}}} \frac{d\tilde{z}}{E(\tilde{z})} \right), \tag{2}$$

where $E(z) \equiv H(z)/H_0$, the curvature density parameter $\Omega_{K,0} \equiv -\kappa c^2/a_0^2 H_0^2$, and sinx is sinh (sin) in the case of $\Omega_{K,0} > 0$ ($\Omega_{K,0} < 0$) and, for $\Omega_{K,0} = 0$ this equation simplifies as the integral. With the denotation of $d(z) \equiv d(0,z)$, Equation (2) links $d_{ls} \equiv d(z_s, z_l)$, $d_s \equiv d(z_s)$, and $d_l \equiv d(z_l)$ in the FLRW metric via the distance sum rule (Räsänen et al. 2015),

$$d_{ls} = \epsilon_1 d_s \sqrt{1 + \Omega_{K,0} d_l^2} - \epsilon_2 d_l \sqrt{1 + \Omega_{K,0} d_s^2}, \tag{3}$$

where $\epsilon_i = \pm 1$ with the positive case is required for the one-to-one correspondence between z and t, with d'(0) > 0. We assume the

case of $\epsilon_i = 1$, then Equation (3) can be rewritten as

$$\frac{d_{ls}}{d_s d_l} = \sqrt{1/d_l^2 + \Omega_{K,0}} - \sqrt{1/d_s^2 + \Omega_{K,0}}.$$
 (4)

Strong lensing systems benefit from their very simple underlying physics and purely gravitational origin compared to the other cosmological probes. The measurement of time delay $\Delta t_{i,j}$ between lensed images i and j at the coordinates θ_i and θ_j and a concrete lens model provide the measurement of time-delay distance $D_{\Delta t}$ through (Refsdal 1964; Schneider et al. 1992)

$$\Delta t_{i,j} = \frac{D_{\Delta t}}{c} \Delta \psi_{i,j},\tag{5}$$

where $\Delta \psi_{i,j} = [(\theta_i - \beta_s)^2/2 - \psi(\theta_i) - (\theta_j - \beta_s)^2/2 + \psi(\theta_j)]$ represents the "Fermat potential" difference between lensed images with the two-dimensional lensing potential ψ and source position β_s . The time-delay distance is the combination of the three angular diameter distances:

$$D_{\Delta t} = (1 + z_l) \frac{D_{A,l} D_{A,s}}{D_{A,ls}} = \frac{c}{H_0} \frac{d_l d_s}{d_{ls}}. \tag{6}$$

Therefore, H_0 and $\Omega_{K,0}$ can be directly determined by comparing Equation (4) with the time-delay distance ratio $d_{ls}/d_s d_l$ extracted from lensing time delay data through Equations (5) and (6).

To reduce the model dependence and take the full advantage of the whole $D_{\Lambda t}$ measurements, we make use of GRBs as distance indicators to derive d_l and d_s out to very high redshifts in Equation (4) via $d(z) = H_0 d_L(z) [c(1+z)]^{-1}$, which holds in any space-time for any gravity theory. Due to the lack of low-z GRBs, we also combine the well-calibrated Pantheon SNe Ia (see Section 3.2) as references to optimize the constraints on d_I and d_S . In principle, one needs to select a pair of SC events that match the redshifts of the lens and source in a lensing system. However, it is difficult for this to be fulfilled with all the discrete data, and there are always differences in the lensing redshifts from the nearest SC objects. This can be resolved by smoothing the evolution of luminosity distances from all discrete events through a model-independent way, for instance, making use of a polynomial (Räsänen et al. 2015) or non-parametric approach like the Gaussian process (Shafieloo et al. 2012). It is worth stressing that, the polynomial $d(z) = \sum_{i=1}^{n} c_i z^i$ conditional on d(0) = 0 and d'(0) = 1 adopted in previous works (e.g., Collett et al. 2019; Wei & Melia 2020) as the parametrization of SC distances might suffer from the divergence and convergence problems when fitting to the highredshift data sets, and the finite truncated polynomials could result in some systematic errors. General cosmography provides an ideal tool to explore the dynamical evolution of cosmic expansion according to the cosmological principle and without specifying a cosmological model, intrinsically owning the idea of fitting data using the Taylor series expanding around $z \approx 0$ with the scale factor derivatives up to a certain order (Visser 2004; Capozziello et al. 2013, 2019; Aviles et al. 2014).

To avoid the convergence and divergence problem mentioned above, we adopt the Taylor series expansions, with the scale factor derivative up to the fourth order, as a function of the y-redshift (Cattoën & Visser 2008), y = z/(1+z), for the SC distance parametrizations (see Capozziello et al. 2013 for more details). In the Appendix,

we define the leading-order cosmographic parameters to be constrained, including the deceleration q_0 , jerk j_0 , snap s_0 parameters, etc., and different distances determined by Taylor series are presented (see Capozziello et al. 2013 for more detailed descriptions about the evolutionary status of the universe corresponding to these parameters). Note that the SC distances encode both the H_0 and $\Omega_{K,0}$ in the cosmography formulae. Thus our method can adequately explore how constraining the H_0 and $\Omega_{K,0}$ are in the DSR approach.

2.2 Bayesian framework

We infer the free parameters within the Bayesian framework (the methods described below are referred to Trotta 2017). Given the observational data, D, and prior knowledge in modelling the SC distance indicators (see Section 3.2) and cosmographic models (i.e., the order of expansions), the posterior probability distribution of the free parameters, θ , is given by

$$p(\boldsymbol{\theta}|\boldsymbol{D}) = \frac{\mathcal{L}(\boldsymbol{\theta}; \boldsymbol{D})\pi(\boldsymbol{\theta})}{\int \mathcal{L}(\boldsymbol{\theta}; \boldsymbol{D})\pi(\boldsymbol{\theta})d\boldsymbol{\theta}}.$$
 (7)

The term $\mathcal{L}(\theta; \mathbf{D}) = p(\mathbf{D}|\theta)$ is the *likelihood* of observational data conditional on the knowledge of such free parameters of hypothetic models, which permits to combine different data sets with the summation of log-likelihoods for the parameter inference. For the *prior* $\pi(\theta)$, we use uniform distributions by taking large and physically acceptable ranges for each free parameter unless specified otherwise, as shown in Table 1. The right-hand-side integral in Equation (7) is the *evidence*.

The marginalized posterior probability distribution of each parameter is obtained with implementing the dynamical nested sampling code dynesty (Speagle 2020)². Dynamical nested sampling has desirable merits over the Markov chain Monte Carlo algorithms with sophisticated treatment of multimodal solutions, more flexible access to independent samples, and in particular, focusing on effectively and simultaneously estimating the posterior and evidence while sampling from complicated, multimodal distributions. Besides, dynamic nested sampling allows samples to be targeted adaptively to better sample specific areas of the posterior during the fit. In this work, for each Bayesian parameter, we report the median of the marginalized posterior probability distribution along with the 1σ error bar taken as half of the 16th-84th quantile range.

3 DATA AND LIKELIHOOD CONSTRUCTIONS

3.1 Strong Lensing Time-Delay Distances

We compile the recent six strongly lensed quasars with time-delay measurements from H0LiCOW collaboration (Wong et al. 2020), including B1608+656 (Suyu et al. 2010; Jee et al. 2019), RXJ1131-1231 (Suyu et al. 2014; Chen et al. 2019), HE0435-1223 (Wong et al. 2017; Chen et al. 2019), WFI2033-4723 (Rusu et al. 2020), J1206+4332 (Birrer et al. 2019), and PG1115+080 (Chen et al. 2019). All lenses except B1608+656 are blindly analyzed with respect to the cosmological parameters. The posterior distributions of time-delay distance of these galaxy lenses are publicly released at the H0LiCOW

¹ Analogous approaches have been proposed to parameterize cosmic distances, such as Padé series (Gruber & Luongo 2014) and Chebyshev polynomials (Capozziello et al. 2018). However, it is very difficult to determine the approximation order due to the dearth of data points and the qualities of cosmological measurements.

https://github.com/joshspeagle/dynesty

website³. For B1608+656, the time-delay distance likelihood function was approximated with a skewed log-normal distribution:

$$\mathcal{L}_{D_{\Delta\tau}} = \frac{1}{\sqrt{2\pi}(x - \lambda_D)\sigma_D} \exp\left[-\frac{(\ln(x - \lambda_D) - \mu_D)^2}{2\sigma_D^2}\right],\tag{8}$$

with the parameters $\mu_D = 7.0531$, $\sigma_D = 0.22824$, and $\lambda_D = 4000.0$, where $x = D_{\Lambda t}$ (in units of Mpc). The time delay posterior distributions of the remaining five lensed quasars were released with the samples of Monte-Carlo Markov Chains. We also include DES-J0408-5354 from STRIDES collaboration (Shajib et al. 2020), which sets the current most precise measurement of H_0 from a single timedelay lens. For this event, we use the time-delay distance posterior distribution derived by Shajib et al. (2020). Besides, SDSSJ0946+1006 (Gavazzi et al. 2008) is a double-source-plane strong lensing with the presence of two sources ($z_{s1} = 0.609$, $z_{s2} = 2.3$) that lensed by the same foreground galaxy ($z_l = 0.222$), offering an accurate constraint on the cosmological scaling factor $\xi = (d_{ls1}d_{s2}/d_{s1}d_{ls2}) =$ $(d_{ls1}/d_ld_{ls1})\cdot(d_ld_{l,s2}/d_{l,s2})$, which is sensitive to $\Omega_{K,0}$ and with no dependence on H_0 . In SDSSJ0946+1006, the constrain result is $\xi^{-1} = 1.404 \pm 0.016$ (Collett & Auger 2014). Thus, we can well approximate the likelihood function $\mathcal{L}_{\mathcal{E}^{-1}}$ using a Gaussian function with the mean value and dispersion $\mu_{\mathcal{E}^{-1}} \pm \sigma_{\mathcal{E}^{-1}} = 1.404 \pm 0.016$,

$$\mathcal{L}_{\xi^{-1}} = \frac{1}{\sqrt{2\pi}\sigma_{\xi^{-1}}} \exp\left\{-\frac{\left[\xi^{-1} - \frac{T(z_l) - T(z_{s2})}{T(z_l) - T(z_{s1})}\right]}{2\sigma_{\xi^{-1}}^2}\right\},\tag{9}$$
with $T(z) = \sqrt{1/d^2(z) + \Omega_{K,0}}$.

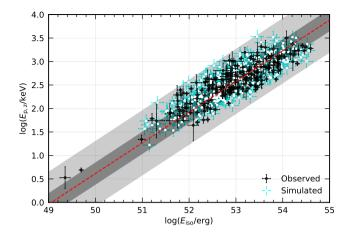
3.2 Distance indicators used to derive d_l and d_s

Gamma-Ray Bursts. We compile 193 redshift-known LGRBs from Amati et al. (2019), and implement the Amati correlation as GRB distance indicators. For this GRB sample, ~ 70% of them lie in the 0.5 < z < 2.5 range with an average of $\bar{z} \sim 1.9$. Similar to Amati et al. (2019), we write the Amati correlation as a power-law function of the cosmological rest-frame peak energy, $E_{p,z}$, derived from the observer-frame one, $E_{p,obs}$, via $E_{p,z} = E_{p,obs}(\hat{1} + z)$, and the prompt γ -ray energy of LGRBs, $E_{\rm iso} = 4\pi d_{\rm L}^2(z, \Omega) S_{\rm bol} (1+z)^{-1}$, where $d_{\rm L}$ is the luminosity distance (in units of cm) in terms of an approximate parametrization or a specific cosmology with free parameters Ω , S_{bol} is the observable bolometric integral flux (in units of erg·cm⁻¹) within the energy band of observing instruments, and the factor (1+z) is the correction of cosmological time dilation effect. Taking the logarithm, the $E_{p,z}$ – E_{iso} correlation can be modelled as

$$\log(E_{\rm iso}/{\rm erg}) = A + B \log(E_{\rm p,z}/{\rm keV}), \tag{10}$$

with the constants A and B being the coefficient values of Amati correlation. Equation (10) links the theoretical distance $d_{\rm L}(z, \Omega)$ to the observable sets $\{z, E_{p,z}, S_{bol}\}$ of LGRB population. Then the likelihood function is given such that

$$\mathcal{L}_{grb} = \prod_{i=1}^{193} \frac{1}{\sqrt{2\pi(\sigma_{\log(S_{bol}),i}^{2} + B^{2}\sigma_{\log(E_{p,z}),i}^{2} + \delta_{grb}^{2})}} \times \exp\left[-\frac{\Delta_{grb,i}^{2}}{2(\sigma_{\log(S_{bol}),i}^{2} + B^{2}\sigma_{\log(E_{p,z}),i}^{2} + \delta_{grb}^{2})}\right], \tag{11}$$



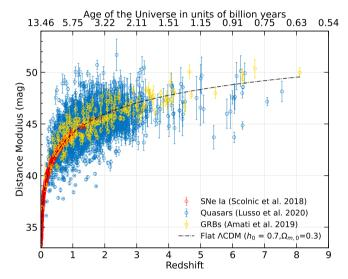


Figure 1. Upper panel: The derived best-fitting $E_{p,z} - E_{iso}$ relation assuming a flat Λ CDM cosmology with taking $H_0 = 70 \text{ km} \cdot \text{s}^{-1} \cdot \text{Mpc}^{-1}$ and $\Omega_{\text{m.0}} =$ 0.3 (red dashed line), $1\delta_{grb}$ (dark gray) and $3\delta_{grb}$ (light gray) confidence regions. The black symbols are the observed data and the cyan points denote the simulated (see section 4.2). Lower panel: The Hubble diagrams of the standardizable candles implemented in this work, including SNe Ia (red), quasars(blue), and GRBs(orange). Note that we adopt the quasars with $z \le 5$ for our analysis in this work (see Section 3.2). The term $h_0 = H_0/(100 \text{ km} \cdot \text{m})$ $s^{-1} \cdot Mpc^{-1}$).

and

$$\Delta_{\rm grb} = \log(S_{\rm bol}) - A - B \, \log(E_{\rm p,z}) + \log(4\pi d_{\rm L}^2/(1+z)), \eqno(12)$$

Here, $\sigma_{\log E_{\rm p,z}}$ ($\sigma_{\log S_{\rm bol}}$) represents the error propagation (in logarithm) of the observed $E_{\rm p,z}$ ($S_{\rm bol}$), $\delta_{\rm grb}$ is a free parameter accounting for the intrinsic dispersion around the best-fitting relation of Equation (10). Throughout we neglect the uncertainties of spectroscopically measured redshift and K-correction for taking into account the cosmological redshifting of the GRB spectra and the limited bandwidth of observing telescopes (Bloom et al. 2001).

In the upper panel of Figure 1, we present the best-fitting $E_{\rm p,z}-E_{\rm iso}$ relation (red dashed line) along with $1\delta_{\rm grb}$ and $3\delta_{\rm grb}$ confidence regions by assuming the flat ACDM as a fiducial cosmology ($H_0 = 70 \text{ km} \cdot \text{s}^{-1} \cdot \text{Mpc}^{-1}$, $\Omega_{\text{m},0} = 0.3$, the same as below), where $A = 49.06 \pm 0.32$, $B = 1.53 \pm 0.12$, and $\delta_{\text{grb}} = 0.35 \pm 0.04$ dex. The derived GRB Hubble diagram is plotted in the lower panel (see

http://www.h0licow.org

Table 1. Priors used in the nested sampling and each free parameter's descriptions. \mathcal{U} represents a uniform probability distribution.

Parameter	Prior	Description of Parameter					
M _B [mag]	U(-25,-15)	B-band absolute peak magnitude of SNe Ia.					
A	U(0,100)	Intercept of the Amati correlation of LGRBs in logarithm.					
B	U(0,5)	Slope of Amati correlation of LGRBs in logarithm.					
$\delta_{ m grb}$	U(0,2)	Intrinsic dispersion of Amati correlation of LGRBs in logarithm.					
$eta^{\ddot{c}}$	U(-5,5)	Parameter related to the intercept (β) of quasar's $L_{\rm X}$ – $L_{\rm UV}$ relation in logarithm					
γ	U(0,2)	Slope of quasar's $L_{\rm X}$ – $L_{\rm UV}$ relation in logarithm.					
$\delta_{ m qso}$	U(0, 2)	Intrinsic scatter of quasar's $L_{\rm X} - L_{\rm UV}$ relation in logarithm.					
H_0 [km·s ⁻¹ ·Mpc ⁻¹]	U(40, 90)	Present cosmic expansion rate.					
$\Omega_{K,0}$	U(-1, 1)	Present energy density of spatial curvature component.					
q_0	U(-2,0)	Cosmographic deceleration parameter.					
j_0	U(-10,10)	Cosmographic jerk parameter.					
s_0	U(-150,150)	Cosmographic snap parameter.					

Table 2. The bounds obtained with different independent data combinations at 1σ credibility.

Data combined	H_0^*	$\Omega_{K,0}$	q_0	j_0	s_0	M_B	A/γ	B/β'	$\delta_{ m grb}/\delta_{ m qso}$
Lensing+SN Ia	75.8+3.7	$0.12^{+0.16}_{-0.14}$	$-0.64^{+0.24}_{-0.25}$	$2.6^{+3.9}_{-4.1}$	$1^{+48}_{-27} \\ -6^{+39}_{-25}$	$-19.17^{+0.09}_{-0.08}$			
Lensing+SN Ia+SH0ES	$74.2^{+0.5}_{-1.4}$	$0.12^{+0.10}_{-0.14}$ $0.04^{+0.10}_{-0.10}$	0.50+0.25	$1.0^{-4.1}_{-3.6}$	-6^{+39}_{-25}	10 24+0.04			
Lensing+SN Ia+ H_0^*	$76.6^{+2.5}_{-2.7}$	$0.11^{+0.16}_{-0.11}$	0.60±0.29	$2.7^{+3.7}_{3.0}$	-6^{+35}_{-25} 6^{+42}_{-31}	$-19.24^{+0.05}_{-0.02}$ $-19.14^{+0.05}_{-0.09}$			
Lensing+SN Ia	$73.8^{+2.3}_{-1.8}$	flat	0 (1+0) 23	$2.1^{+3.6}_{-4.7}$	-22^{+61}_{-12}	$-19.24^{+0.06}_{-0.05}$			
Lensing+QSO	$77.6^{+2.8}_{-3.3}$	$-0.21^{+0.41}_{-0.49}$	0.41 ± 0.28	$6.3^{-4.7}_{-2.7}$	34^{+412}_{-35} 34^{+34}_{-40}	-0.03	$0.58^{+0.01}_{-0.01}$	$-1.63^{+0.04}_{-0.02}$	$0.22^{+0.01}_{-0.01}$
Lensing+QSO+ H_0^*	77 0+2.6	$-0.21^{+0.149}_{-0.49}$ $-0.23^{+0.38}_{-0.50}$	0.27+0.26	$7.6^{+1.8}_{-4.5}$	34^{+34}_{40}		$0.58_{-0.01}^{+0.01}$ $0.58_{-0.01}^{+0.01}$	1 (2+0.04	$0.22_{-0.01}^{+0.00}$ $0.22_{-0.00}^{+0.00}$
Lensing+QSO	77.9+2:8	flat	0.45+0.34	$7.2^{+2.3}_{-3.7}$	18^{+48}_{-20}		$0.58_{-0.01}^{+0.01}$ $0.58_{-0.01}^{+0.01}$	$-1.62^{+0.03}_{-0.02}$	0.22+0.01
Lensing+GRB	$71.5^{+4.4}_{-3.0}$	$-0.07^{+0.13}_{-0.06}$	0.20+0.11	$-1.4^{+5.2}_{-4.9}$	96+44		40 40±0 17	$1.47^{+0.06}_{-0.08}$	$0.37^{+0.02}_{-0.02}$
Lensing+GRB+ H_0^*	$72.9^{+3.1}_{-3.0}$	$-0.07_{-0.06}$ $-0.02_{-0.07}^{+0.17}$	0.60±0.43	$0.4^{+4.6}_{-5.1}$	56 ⁺⁵⁹		$49.19^{+0.17}_{-0.18}$ $49.20^{+0.17}_{-0.17}$	$1.46^{+0.07}_{-0.07}$	$0.37^{+0.02}_{-0.02}$
Lensing+GRB	$70.9^{+4.2}_{-2.9}$	flat	0.42+0.33	$-0.4^{+3.8}_{-5.2}$	201/16		40.21+0.15	1 47+0.06	$0.37^{+0.03}_{-0.02}$
Lensing+GRB [†]	$70.4_{-3.3}^{-2.9}$	$-0.07^{+0.03}_{-0.02}$	0.40±0.37	$-3.3^{+3.4}_{-4.6}$	440+37		$49.21_{-0.20}$ $49.31_{-0.13}^{+0.10}$	$1.47^{+0.04}$	$0.27^{+0.01}_{-0.02}$
Lensing+GRB † + H_0^{\star}	$71.4^{+3.2}_{2.8}$	$-0.07_{-0.02}^{+0.03}$ $-0.07_{-0.02}^{+0.03}$		$-3.8^{+4.6}_{-3.9}$	112^{+37}_{-72}		40.31+0.11	$1.47^{+0.03}_{-0.05}$	$0.27^{+0.01}_{-0.02}$
Lensing+GRB [†]	60 0+3.0	flat	0.00+0.78	$-2.3^{+3.1}_{-3.2}$	122+16		$49.23^{+0.12}_{-0.09}$	$1.47^{+0.04}_{-0.04}$	$0.27^{+0.02}_{-0.02}$
Lensing+SN Ia+QSO	$78.0^{+2.9}_{-3.0}$	$0.14^{+0.16}_{-0.15}$		$8.9_{-2.7}^{+1.0^{2}}$	133 ⁺ 50 96 ⁺ 12 96 ⁺ 39 61 ⁺ 24 86 ⁺ 22 -31	$-19.14^{+0.09}_{-0.07}$	0.00+0.01	$-1.56^{+0.01}_{-0.02}$	$0.27_{-0.02}$ $0.22_{-0.00}^{+0.00}$ $0.22_{-0.00}^{+0.00}$
Lensing+SN Ia+QSO+SH0ES	$74.1^{+0.8}_{-1.0}$	0.01+0.10	0.00 ± 0.20	$7.8^{+1.8}_{-3.6}$	61^{+24}_{-34}	10 24+0.03	0.60 + 0.00	1 5 4+0.01	$0.22^{+0.00}_{-0.00}$
Lensing+SN Ia+QSO+H ₀ [⋆]	$77.0_{-2.4}^{+2.7}$	$0.01_{-0.10}^{-0.10}$ $0.11_{-0.14}^{+0.15}$	0.01+0.13	$8.5^{+1.4}_{-2.5}$	86^{+22}_{-31}	10.26+0.01	0.60+0.00	1 50+0.01	$0.22_{-0.00}^{+0.00}$ $0.23_{-0.00}^{+0.00}$
Lensing+SN Ia+QSO	$75.4_{-1.8}^{+2.3}$	flat	0 00+0.tg	0.1+0.9	99+10	10 20+0 05	18.8		$0.22^{+0.00}_{-0.00}$
Lensing+SN Ia+GRB	$75.6^{+3.3}_{-2.9}$	$0.10^{+0.18}_{-0.12}$	0.50+0.23	$0.7^{+3.7}_{-3.5}$	-10^{+40}	10 10+0.09	$49.15^{+0.15}_{-0.20}$	$1.38^{+0.07}$	$0.38^{+0.02}_{-0.02}$
Lensing+SN Ia+GRB+SH0ES	$74.0_{-1.1}^{+0.7}$	$0.04^{+0.11}_{-0.08}$	0.42+0.19	$-0.5^{+3.3}_{-2.9}$	-9_{-24}^{-22}	10 22+0.07	40 4 = +() 16	$1.39^{+0.06}$	$0.38^{+0.02}_{-0.02}$
Lensing+SN Ia+GRB+H ₀ [⋆]	$75.3^{+3.0}_{-2.5}$	$0.04^{+0.08}_{-0.08}$ $0.10^{+0.16}_{-0.12}$		$-1.2^{+4.8}_{-2.0}$	-9_{-24} -17_{-17}^{+38}	10 10+0 08	49.15-0.18 49.12-0.17	$1.40^{+0.05}$	$0.38^{+0.02}_{-0.02}$
Lensing+SN Ia+GRB	$73.3^{+2.2}_{-1.8}$	flat		$-0.8^{+3.8}_{-3.7}$	-23^{+38}_{-18}	10 22+0.04	40 47+0 15	$1.38^{+0.08}_{-0.06}$	$0.38_{-0.02}^{+0.02} \ 0.38_{-0.03}^{+0.02}$
Lensing+SN Ia+GRB [†]	$74.6^{+2.5}_{-2.9}$	$0.07^{+0.14}_{-0.12}$	U 33+0.10	$-4.4^{+2.7}_{-2.0}$	-31^{+16}_{-15}	10 10+0 05	18 08+0.11	1 45+0.05	0.20 ± 0.02
Lensing+SN Ia+GRB [†] +SH0ES	$73.5^{+1.1}_{-0.8}$	$0.07_{-0.12}$ $0.04_{-0.08}^{+0.1}$	0.10+0.12	$-4.6^{+2.6}_{-1.7}$	-30^{+14}_{-16}	10 22+0.02	49 00+0.10	$1.43_{-0.03}$ $1.47_{-0.04}^{+0.04}$	$0.29^{+0.01}_{-0.01}$ $0.29^{+0.02}_{-0.01}$
Lensing+SN Ia+GRB † + H_0^{\star}	$73.3_{-0.8}^{+0.8}$ $74.8_{-2.8}^{+2.3}$	$0.04^{+0.08}_{-0.08}$ $0.09^{+0.12}_{-0.14}$	0.17+0.09	$-4.1^{-2.3}_{-2.1}$	-30^{-16}_{-16} -32^{+16}_{-14}	40 20±0 07	40.00+0.11	$1.47_{-0.04}^{+0.04}$ $1.46_{-0.04}^{+0.04}$	0.20+0.02
Lensing+SN Ia+GRB [†]	$73.2_{-1.8}^{-2.8}$	flat	$-0.17^{+0.02}_{-0.22}$ $-0.19^{+0.13}_{-0.20}$	$-4.4^{+2.0}_{-2.4}$	-32^{+10}_{-14} -35^{+14}_{-14}	$-19.20^{+0.08}_{-0.08}$ $-19.24^{+0.04}_{-0.06}$	$49.00^{+0.11}_{-0.11}$	$1.46^{+0.04}_{-0.04}$ $1.46^{+0.04}_{-0.04}$	$0.29_{-0.02}^{+0.02} \\ 0.29_{-0.02}^{+0.02}$

orange points). One can see that the GRBs distance moduli are consistent with the SN Ia ones at low redshifts ⁴, albeit with an intrinsic dispersion of around 0.35 dex in logarithmic space. Besides, Demianski et al. (2021) parametrized the redshift evolution of Amati parameters in the form of a power-law function and showed that there is no significant trend systematic with redshift for the observables, coefficients, as well as δ_{grb} , by cross-comparing the calibrations in different redshift bins and observing instruments using a local regression technique. Therefore, we can safely use this sample of LGRBs as distance indicators.

Pantheon Supernovae Ia. The Pantheon compilation released the current most complete SN Ia sample, which consists of 1048 objects covering the redshift range of $0.01 \le z \le 2.3$ (Scolnic et al. 2018). As shown in the lower panel of Figure 1, most of the SN Ia events ($\sim 80\%$) are located in the redshift range 0.2 < z < 0.6, and only 6 of them are at z > 1.4, much insufficient to be used to cover the redshift range of current strong lensing systems. The observed SN Ia distance moduli (red points in this panel) are calculated from the Spectral

^{*} In units of km·s⁻¹·Mpc⁻¹.

*With using $H_0 = 74.5^{+5.6}_{-6.1}$ km·s⁻¹·Mpc⁻¹ as a prior.

[†] With 500 mock GRBs combined.

⁴ The absolute magnitude of all SN Ia objects is fixed to -19.35 mag, which corresponds to $H_0 = 70 \text{ km} \cdot \text{s}^{-1} \cdot \text{Mpc}^{-1}$, see Scolnic et al. (2018).

Adaptive Light curve Template 2 (SALT2) light-curve fit parameters with using a modified version of the Tripp formula (Tripp 1998):

$$\hat{\mu}_{\text{obs}} = m_{\text{B}} - M_{\text{B}} + \alpha \cdot X - \eta \cdot C + \Delta_{\text{M}} + \Delta_{\text{B}}, \tag{13}$$

where $m_{\rm B}$ is the B-band apparent magnitude, X is the stretch factor, C is the color parameter, α and η are the nuisance coefficients of the stretch- and color-luminosity relations, respectively, and $M_{\rm B}$ is another nuisance parameter that represents the B-band absolute peak magnitude of a fiducial SNe Ia with X = 0 and C = 0. Furthermore, Δ_{M} and Δ_B are the distance corrections based on the host-galaxy mass and from various biases predicted from simulations, respectively. For the Pantheon SNe Ia, the values of α and η are calibrated by using the Bayesian Estimation Applied to Multiple Species with Bias Corrections (BBC) method (Kessler & Scolnic 2017), whistle correcting those expected biases (See Marriner et al. 2011 for more details.). With the BBC technique, Scolnic et al. (2018) reported the apparent magnitudes with bias corrections (m_{corr}) of all SNe Ia. Then the observed distance modulus is given by directly subtracting $M_{\rm B}$ from m_{corr} , i.e., $\hat{\mu}_{\text{obs}} = m_{\text{corr}} - M_{\text{B}}$. Using the vector of SN distance residuals $\Delta \mathbf{m} = \hat{\boldsymbol{\mu}}_{\text{obs}} - \hat{\boldsymbol{\mu}}_{\text{model}}$, the likelihood function of the model

$$-2\ln(\mathcal{L}_{sn}) = \Delta \mathbf{m}^T \cdot \mathbf{C}^{-1} \cdot \Delta \mathbf{m}. \tag{14}$$

Here, **C** is the uncertainty matrix (including both statistical and systematic uncertainties), $\hat{\mu}_{\text{obs}}$ and $\hat{\mu}_{\text{model}}$ are respectively the observed and model vector of SN distance moduli with $\hat{\mu}_{\text{model}} = 5 \log[d_{\text{L}}(z, \mathbf{\Omega})/(10 \text{ pc})]$.

Actually, in our method SN Ia data can be anchored near their high-redshift end in combination with $D_{\Delta t}$ measurements from TDGLs (Taubenberger et al. 2019; Wong et al. 2020), thus we do not take a fiducial value of H_0 in SN Ia distances in our fitting.

Quasar Sample. Quasars are of high luminosity emerging at galaxy scales and have served as a new cosmological probe of the high-redshift universe (Risaliti & Lusso 2019; Lusso et al. 2020). Recently, Lusso et al. (2020) reported a new catalogue of 2421 optically selected quasars with the measurements of spectroscopic redshifts and X-ray observations from either Chandra or XMM-Newton. This high-quality sample enables set up the Hubble diagram up to redshift $z \sim 7.5$ by using the non-linear phenomenological relation between the X-ray and ultraviolet luminosities of quasars (Avni & Tananbaum 1982; Lusso & Risaliti 2017), written logarithmically as

$$\log L_{\rm X} = \beta + \gamma \log L_{\rm UV},\tag{15}$$

where $L_{\rm X}$ and $L_{\rm UV}$ correspond to the monochromatic luminosities at 2 keV and 2500, respectively. Then the distance indicator of quasars can be re-expressed as a function of the UV and X-ray fluxes (both in units of erg cm⁻² s⁻¹ Hz⁻¹), $F_{\rm UV}$ and $F_{\rm X}$, luminosity distance, $d_{\rm L}$ at redshift z, i.e.,

$$\log F_{\rm X} = \beta + \gamma \log F_{\rm UV} + (\gamma - 1) \log 4\pi d_{\rm I}^2(z). \tag{16}$$

We can obtain the quasar distances by directly fitting the relation between F_X and F_{UV} as a function of the slope γ and intercept β . The redshift dependence of γ and β has been evaluated in a cosmology-independent way by using sub-samples in narrow redshift bins. With this approach, Lusso et al. (2020) verified that both γ and β do not show significant trend with redshift at $z \leq 5$. We thus use 2404 quasars with redshift $z \leq 5$ in the following analyses. It should be noted that the intercept β is very difficult to be determined due to the lack of confident physical interpretations for the $L_X - L_{UV}$ relation as well as its intrinsic dispersion, $\delta_{\rm qso}$. Therefore, we set γ , β , and $\delta_{\rm qso}$ as free parameters to be marginalized over in our fitting, which can also partly alleviate the problem of the mismatch in the shape of

Hubble diagrams of quasars and other probes (e.g., the SNe Ia). The quasar likelihood function is given by

$$\mathcal{L}_{qso} = \prod_{i=1}^{2404} \frac{1}{\sqrt{2\pi(\sigma_{\log(F_{X}),i}^{2} + \gamma^{2}\sigma_{\log(F_{UV}),i}^{2} + \delta_{qso}^{2})}} \times \exp\left[-\frac{\Delta_{qso,i}^{2}}{2(\sigma_{\log(F_{X}),i}^{2} + \gamma^{2}\sigma_{\log(F_{UV}),i}^{2} + \delta_{qso}^{2})}\right], \tag{17}$$

and

$$\Delta_{\text{qso}} = \log(F_{\text{X},30}) - \beta' - \gamma \log(F_{\text{UV},27.5}) - 2(\gamma - 1) \log(d_{\text{L},28.5}(z, \mathbf{\Omega})),$$
(18)

where $\beta' = \beta + (\gamma - 1) \log(4\pi)$, F_X and F_{UV} are normalised (in logarithm) to 30 and 27.5, respectively.

The lower panel of Figure 1 also displays the quasar Hubble diagram (blue symbols), which is derived by fitting the data with fifth-order logarithmic polynomials (Lusso et al. 2020). We can see that quasars exhibit a relatively large dispersion and appear to deviate from the flat Λ CDM beyond $z\sim 2$ (see Lusso et al. 2020 for more details). We thus focus on the cosmographic fits with the combined $D_{\Delta t}$ of TDGLs, SN Ia, and GRB data. Nevertheless, the combined results with quasars can be employed for comparison and validation in our model-independent measurements.

4 RESULTS AND DISCUSSIONS

4.1 Current observational constraints

We first focus on the cosmographic fits by combining TDGLs, SNe Ia, and GRBs. For all the free parameters, we use uninformative priors, in particular, for the cosmographic parameters, we adopt the priors used by Li et al. (2020). In Table 1, we give the priors and detailed descriptions of each free parameter to be constrained. Table 2 tabulates the best-fitting results and 1σ credible intervals produced from a random sampling of the Bayesian formulae using the dynamic nested sampling code. We display the 1σ and 2σ marginalized posterior probability distributions (contours) in the cornerplots of Figure 2. Combining the lensing and low-redshift SNe Ia yields $H_0 = 75.8^{+3.7}_{-2.5} \text{ km s}^{-1} \text{Mpc}^{-1} \text{ and } \Omega_{K,0} = -0.12^{+0.16}_{-0.14}, \text{ with smaller}$ statistical uncertainties compared to previous results (Collett et al. 2019), which can be attributed to the fact that the constraints of H_0 and $\Omega_{K,0}$ are contributed by both the $D_{\Delta t}$ and SC distances. This also suggests that the cosmographic parametrizations with a spatial curvature component can, in some degrees, consolidate the direct measurements of H_0 and $\Omega_{K,0}$ via the DSR. Taking a flat-universe prior, we obtain $H_0=73.8^{+2.3}_{-1.8}~{\rm km~s^{-1}Mpc^{-1}}$, significantly improved by 38%. From the upper panel of Figure 2, we notice that the degeneracy between M_B and H_0 in SN Ia distances still exists due to the limited constraints on H_0 by current $D_{\Delta t}$ data, which degrades the determinations of H_0 and then $\Omega_{K,0}$ when combining SNe Ia. To reduce such degeneracy effects, we utilize the prior of H_0 with the most recently released measurement by SH0ES team $(H_0 = 73.30 \pm 1.04 \text{ km s}^{-1}\text{Mpc}^{-1}; \text{Riess et al. 2021})$, and find that the $\Delta\Omega_{K,0}$ falls by \sim 40%. From the Lensing+GRB combination, we obtain $H_0 = 71.5^{+4.4}_{-3.0}$ km s⁻¹Mpc⁻¹ and $\Omega_{K,0} = -0.07^{+0.13}_{-0.06}$ providing a 6% precision measurement of H_0 and favoring a flat universe with $\Delta\Omega_{K,0} \approx 0.1$.

The uncertainties of combining Lensing+GRB mainly come from the poor constraints of cosmographic parameters due to the large dispersion of current GRB data. In the case of a flat universe, the

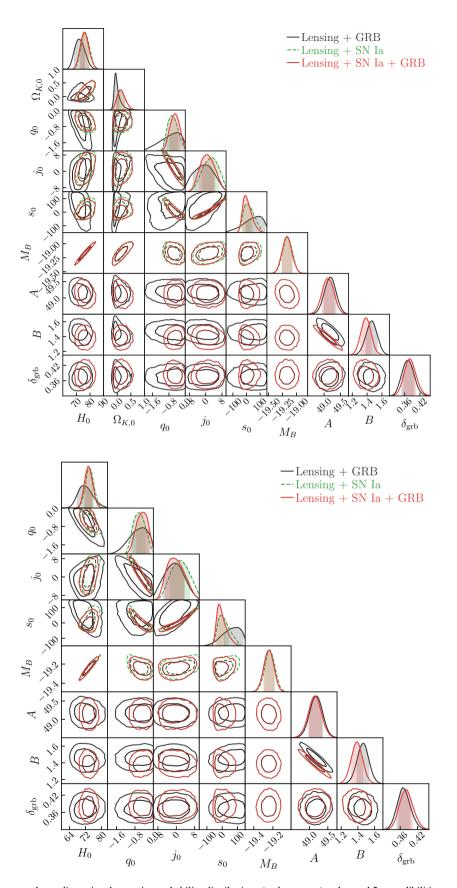
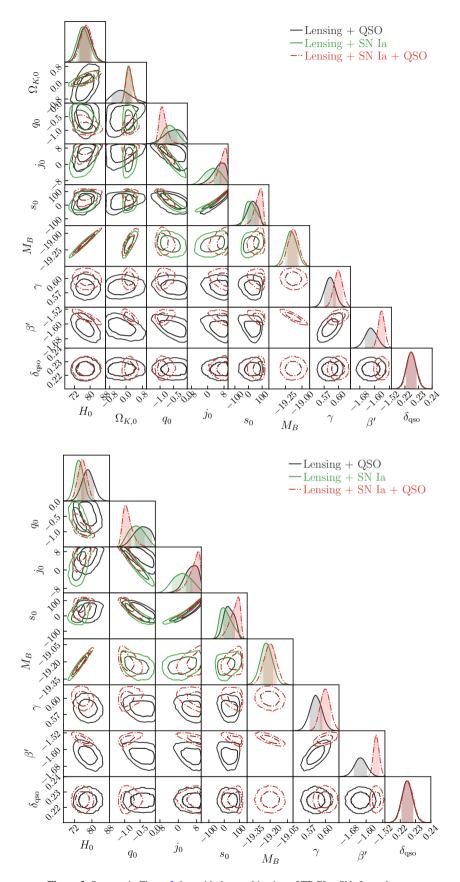


Figure 2. Marginalized one- and two-dimensional posterior probability distributions (and contours) at 1σ and 2σ credibilities produced by dynamical nested sampling with the combination of TDGLs, SNe Ia, and GRBs in general cosmography with a curvature component (upper panel) and with taking a flat universe prior (lower panel).



 $\textbf{Figure 3.} \ \text{Same as in Figure 2, but with the combination of TDGLs, SNe Ia, and quasars.}$

error bar of H_0 is slightly narrowed (by $\sim 5\%$), and the cosmographic parameters are also moderately improved. In addition, the derived values of deceleration, jerk, and snap parameters are in agreement with a present accelerating universe in Λ CDM cosmology, which approximately corresponds to $q_0 \approx -0.55$ ($\Omega_{\rm m,0} = 0.3$), $j_0 = 1$, and $s_0 \approx 0$ (Capozziello et al. 2013), although s_0 is poorly constrained.

SN Ia data possess much better qualities at relatively low redshifts relative to GRBs (and quasars), and thus can be implemented as references to calibrate the GRB (quasar) distances in the same redshift range. Adding the SN Ia data into the Lensing+GRBs, we find that the uncertainty of H_0 is narrowed by 25% relative to the value determined by Lensing+GRBs and the H_0-M_B degeneracy can not be improved. The constraint of $\Omega_{K,0}$ is not improved, which could be the result of the effect of H_0-M_B degeneracy in SN Ia distances and the mismatch between SN Ia and GRB Hubble diagram at $z \gtrsim 1.4^5$. Such degeneracy effects can be seen from the result by taking the SH0ES prior on H_0 , which reduces $\Delta\Omega_{K,0}$ by 39%. In our prospects below, we will show the effects of the uncertainties regarding to GRB distances on the measurements of H_0 and $\Omega_{K,0}$ combining a larger sample of realistic GRBs produced based on a Monte-Carlo simulation.

Figure 3 presents the results by combing Lensing, SNe Ia, and quasars; see also Table 2. In the case of Lensing+QSO, we obtain a relatively higher value of H_0 with $\Delta H_0 \approx 3 \text{ km s}^{-1}\text{Mpc}^{-1}$; the spatial curvature density is loosely constrained with $\Delta\Omega_{K,0} \sim 0.5$. Compared to Lensing+GRB, the looser constraint on $\Omega_{K,0}$ comes from that the quasar distances ($z \leq 5$) have a larger dispersion and larger error bars at high redshifts (e.g., $z \gtrsim 2.5$; see the lower panel in Figure 1), which results in larger uncertainties in the measurements of d_l and d_s and then the $\Omega_{K,0}$. Also, GRB distances have a wider available redshift coverage than the current quasars, which can provide more meaningful constraints. Taking a flat-universe prior gives only a slightly improved value of H_0 . When adding SN Ia data into Lensing+QSO, we obtain only a slight improvement on the limit of H_0 , whereas the $\Delta\Omega_{K,0}$ can be reduced by a factor of 3. While the cosmographic parameters are more constraining relative to Lensing+SN Ia/OSO, their values deviate from that of ΛCDM cosmology at beyond 1σ credible intervals. Meanwhile, compared to the results combining GRB distances above, the outcomes with QSOs also suffer from the $M_B - H_0$ degeneracy in fitting SN Ia distances and the mismatch between SN Ia and QSO Hubble diagrams. Therefore, one should be careful when combining quasar data as complementary distance indicators. The flat-universe assumption provides a 21% reduction for the error bar of H_0 . When imposing the SH0ES prior on H_0 , we obtained a precision similar to the SN Ia and GRB yields.

When adding GRBs to Lensing+SN Ia+QSO, we find no systematic deviation between QSO and GRB distances. There is no significant improvement in our results ($H_0 = 77.4^{+2.9}_{-3.0} \, \mathrm{km \ s^{-1} Mpc^{-1}}$ and $\Omega_{K,0} = 0.13^{+0.17}_{-0.13}$) compared to Lensing+SNIa+QSO and/or Lensing+SNIa+GRB. The result could be due to the mismatch between the SN Ia and GRB/QSO distances, which is a sign of some systematic errors in QSO/GRB distance calibration as using the current $D_{\Delta t}$ measurements for the anchoring along with using SN Ia distances as a reference. Such uncertainties can be further analyzed by using more high-quality time-delay lensing systems, as which "govern" the precision and accuracy in restricting the H_0 . Also, high-quality and large-statistics SNIa/GRB data sets are needed to find out the underlying systematical effects.

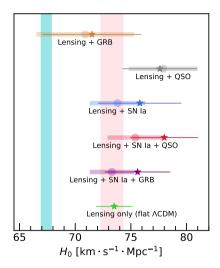


Figure 4. The present values of Hubble parameter determined with different data combinations. The thin and shaded lines denotes the 1σ results with taking a uninformative prior and flat-universe prior on $\Omega_{K,0}$, respectively. The cyan shaded region denotes the CMB (early-universe) measurement in flat Λ CDM cosmology ($H_0 = 67.4 \pm 0.5 \text{ km} \cdot \text{s}^{-1} \cdot \text{Mpc}^{-1}$, Planck Collaboration et al. 2020) and the pink shaded region shows the (late-universe) determination by local distance ladder ($H_0 = 73.30 \pm 1.04 \text{ km} \cdot \text{s}^{-1} \cdot \text{Mpc}^{-1}$, Riess et al. 2021).

In Figure 4, we also display the measurements of H_0 with different data combinations. The value with combining Lensing+GRB is between the CMB and SH0ES results with a precision of $\sim 6\%$ (see Table 2). The Lensing+SN Ia combination results in a value favoured by the SH0ES measurement (pink shaded region) with a $\sim 3\%$ precision in a flat universe. However, the combinations of quasars give a relatively high expansion rate. When combining with SNe Ia, the values coincide with the SH0ES measurement as well as the lensing-only result in a flat Λ CDM cosmology (73.5 ± 1.6 km·s $^{-1}$ ·Mpc $^{-1}$ from this work, see the green symbol) at 1σ credible regions.

In our method, the constraints of H_0 and $\Omega_{K,0}$ rely on the d_l and d_s provided by anchoring the pairs of SC objects on the $D_{\Delta t}$ along with their wide redshift coverage. The measurement of $D_{\Delta t}$ depends on the assumption in lens modelling, which dominates the source of systematic uncertainty in measuring H_0 in time-delay cosmography. Birrer et al. (2020) considered the mass-sheet transformations and obtained $H_0 = 74.5^{+5.6}_{-6.1}~{\rm km~s^{-1}Mpc^{-1}}$. We also use this value as a prior to see the impact of the systematic effects arising from lens modelling on the limit of $\Omega_{K,0}$. The results are presented in Table 2. One can see that such effects do not significantly influence the bound of $\Omega_{K,0}$.

4.2 Future prospects

As shown above, the determinations of H_0 and $\Omega_{K,0}$ via the DSR suffer from the lack of low-redshift GRB observations and the large intrinsic dispersion in the GRB Hubble diagram. Such uncertainties, as well as the effect of M_B-H_0 degeneracy in fitting SN Ia distances, can be improved with larger statistics of GRB data, although the measurement of H_0 is mainly determined by the lensing $D_{\Delta t}$ measurements. Here we perform a Monte-Carlo simulation to investigate the constraints on the cosmographic and spatial curvature parameters by combining the current lensing, Pantheon SN Ia sample, and future GRB observations of the Amati quantities. Our

⁵ This can be seen from the constrained values of the slope *B* and snap parameter between Lensing+GRB and Lensing+SN Ia+GRB, see Table 2.

simulation procedure for producing the z, $E_{p,z}$, and S_{bol} of each GRB event is as follows. First, we fit the gamma distribution function to the current spectroscopic redshift data set, and randomly sample the redshifts in the range 0.001 < z < 2.5, which well covers the current lensing systems. Second, we fit the gaussian function to the $\log(E_{\rm p,z}/{\rm keV})$ data, which gives a mean 2.57 and width 0.45, and $\log(E_{p,z}/\text{keV})$ of each mock GRB is randomly drawn with subject to such a density function. Third, we produce the mock E_{iso} samples using the best-fitting Amati correlation in Equation (10) with considering an intrinsic dispersion $\delta_{grb} = 0.3$ dex, which are determined in a flat ACDM cosmology (see Section 3.2). The jet collimated corrections of the GRB prompt γ -ray energy are neglected, despite the arguments that the jet opening angles could be narrow as below 10 degrees (e.g., Goldstein et al. 2016). Finally, we calculate the mock S_{bol} data from the simulated E_{iso} by evaluating the luminosity distances assuming a flat ACDM model and select the GRB events with a moderate detector threshold of 1×10^{-7} erg cm⁻² (e.g., at the energy band 20-2000 keV). We specify a common statistical uncertainty of 30% for the simulated samples of $\{E_{p,z}, S_{bol}\}$. By running the Monte-Carlo simulation, we produce 500 realistic GRB events for our following analysis⁶, which are shown in the upper panel of Figure 1 (cyan pints).

Figure 5 presents the results by combining the 500 mock GRB events. The 1σ credible intervals are also summarized in Table 2. We find that the restrictions of cosmographic parameters are more stringent compared to that with the real data and the $\Delta\Omega_{K,0}$ can be reduced to ~ 0.02 by using Lensing+mock GRB. The case of using a flat-universe prior further reduces the error bar of H_0 by 14% and results in a 4% precision. When adding the mock GRBs into Lensing+SN Ia, the M_B-H_0 degeneracy can be moderately eliminated (the contours in the M_B-H_0 plane are narrowed and the correlation between M_B and H_0 tends to be weaker) and both the uncertainties of H_0 and H_0 are narrowed compared to Lensing+SN Ia and/or Lensing+SN Ia+GRB. Using the prior of H_0 informed by SH0ES, we can further eliminate the H_B-H_0 degeneracy in SN Ia distances and the result of H_0 is more constraining. In the assumption of a flat universe, the precision of H_0 can reach $\sim 2\%$.

5 SUMMARY

We have provided new independent constraints on the H_0 and $\Omega_{K,0}$ combining the $D_{\Delta t}$ measurements from TDGLs and GRB luminosity distances, only based on the validity of the FLRW metric and geometrical optics. This method benefits from the wide redshift coverage of the absolute distances of lensing systems by using the high-redshift LGRBs, taking the full advantage of $D_{\Delta t}$ measurements in determining H_0 . We use the Amati correlation with 193 redshift-known LGRBs to establish the GRB Hubble diagram up to $z \sim 8.1$, much higher than that of SNe Ia or quasars. The H_0 and $\Omega_{K,0}$ are determined by fitting the $D_{\Delta t}$ and GRB distance indicators through the DSR, in which the GRB distances are parametrized using the general cosmographic parameters together with a curvature component. Thus the limitations of H_0 and $\Omega_{K,0}$ are contributed by both the combined $D_{\Delta t}$ and SC distances.

We present our main findings below. With the combination

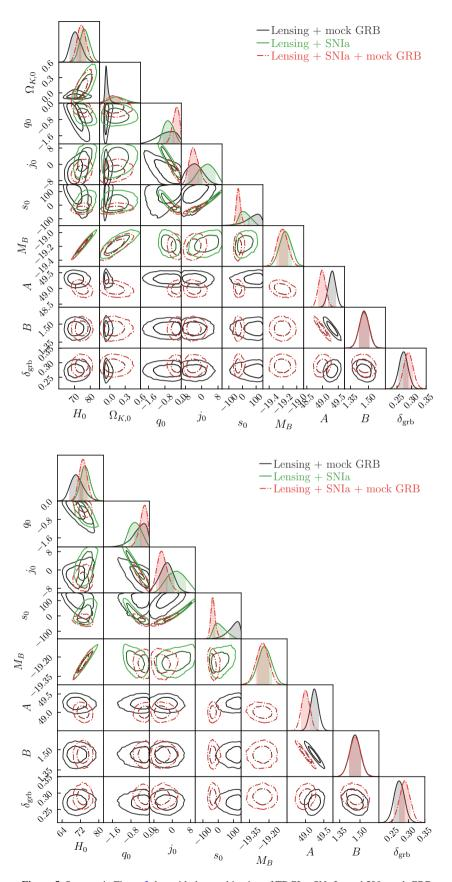
of Lensing+GRB, we obtain $H_0 = 71.5^{+4.4}_{-3.0} \text{ km s}^{-1}\text{Mpc}^{-1}$ and $\Omega_{K,0} = -0.07^{+0.13}_{-0.06}$. In a flat universe, the H_0 is measured to be $H_0 = 70.9^{+4.2}_{-2.9} \text{ km s}^{-1} \text{Mpc}^{-1}$, with a 6% precision. The SN Ia distances can be anchored near their high redshift end in the combination of Lensing+SN Ia, in which the constraints of H_0 and $\Omega_{K,0}$ suffer from the $M_B - H_0$ degeneracy in SN Ia distances due to the limited precision of H_0 provided by $D_{\Delta t}$ measurements of only six TDGLs. In the combination of Lensing+SN Ia+GRB, current GRB data can neither eliminate the $M_B - H_0$ degeneracy when fitting to SN Ia distances nor effectively improve the constraint on H_0 ; the mismatch between the SN Ia and GRB Hubble diagrams due to some systematic errors in the GRB distance calibration contributes to a part of uncertainty in restricting $\Omega_{K,0}$. We performed a Monte-carlo simulation to produce a larger sample of realistic GRBs, and showed that current Lensing+mock GRB could yield inspiring improvements in measuring H_0 (with 4% precision) and $\Omega_{K,0}$ (with an uncertainty of ~ 0.02). Future increment of GRB observations could help eliminate the $M_B - H_0$ degeneracy in SN Ia data and reconcile the SN Ia and GRB Hubble diagrams in the combination of Lensing+SN Ia+GRB, providing more constraining results of H_0 and $\Omega_{K,0}$. In addition, we only include one double-source-plane strong lensing system in our sample, which provides an accurate measurement of the cosmological scaling factor that is sensitive to the value of $\Omega_{K,0}$. The inclusion of more such events will further improve the restrictions on $\Omega_{K,0}$. In contrast, the resultant values of $\Omega_{K,0}$ by using quasars are not very constraining compared to SNe Ia and/or GRBs in conjunction with TDGLs, although they have relatively large statistics. In the combinations with current lensing, SNe Ia, and GRB data sets, we find no evidence of significant deviation from a zero spatial curvature or an accelerating universe, and the values of H_0 coincide with the result of local distance ladder with the best accuracy $\Delta H_0 \approx 2.0$ km $s^{-1}Mpc^{-1}$ (3% precision) in a flat universe.

To date, various solutions for the H_0 tension between the CMB and local measurements (e.g., any new pre-combination physics or the modification of the post-combination expansion history of the Universe) are unlikely to be successful (see e.g., Knox & Millea 2020 and reference therein). In addition, various independent measurements might suffer from some unknown systematic effects (see a recent review by Di Valentino et al. 2021). More precise, model-independent measurements of H_0 and $\Omega_{K,0}$ via the DSR with the increases in the number of time-delay lensing systems (in which more sophisticated lens modelling are expected) and in the statistics of reliable standardizable candles are admired for verifying and providing some clues to the solution of the H_0 tension. Such measurements also give clues to the nature of dark energy and provide a consistency test of the classical FLRW metric.

ACKNOWLEDGEMENTS

We thank the referee for very helpful comments and suggestions. We are grateful to L. Amati for providing the GRB data and Elisabeta Lusso for sharing their latest released quasar sample. Z.-H. Zhu is supported by the National Natural Science Foundation of China under Grants Nos. 12021003, 11920101003 and 11633001, and the Strategic Priority Research Program of the Chinese Academy of Sciences, Grant No. XDB23000000. J.-J. Wei is supported by the NSFC under grant No. U1831122, the Key Research Program of Frontier Sciences (grant No. ZDBS-LY-7014) of Chinese Academy of Sciences, and the Natural Science Foundation of Jiangsu Province (grant No. BK20221562). E.-W. Liang is supported by the National Natural Science Foundation of China (grant Nos. 12133003). Z.-C.

⁶ The expected number of GRBs observed at the design sensitivities of current (Swift, Gehrels et al. 2004; and Fermi, Meegan et al. 2009) and future (SVOM, Götz et al. 2009; LOFT, Feroci et al. 2012; and THUSEUS, Amati et al. 2018) missions dedicated to observing GRBs in the coming decade's operations can reach \sim 600.



 $\textbf{Figure 5.} \ \text{Same as in Figure 2, but with the combination of TDGLs, SNe Ia, and 500 mock GRBs.}$

DATA AVAILABILITY

The data of strong lensing systems we use are available at http: //www.h0licow.org. The GRB and quasar sample are shared on reasonable requests to Amati et al. (2019) and Lusso et al. (2020), respectively. The PYTHON/JUPYTER notebook to reproduce the results of this article will be shared on reasonable request to the corresponding author.

```
REFERENCES
Amati L., 2006, MNRAS, 372, 233
Amati L., et al., 2002, A&A, 390, 81
Amati L., Guidorzi C., Frontera F., Della Valle M., Finelli F., Landi R.,
    Montanari E., 2008, MNRAS, 391, 577
Amati L., et al., 2018, Advances in Space Research, 62, 191
Amati L., D'Agostino R., Luongo O., Muccino M., Tantalo M., 2019, MN-
    RAS, 486, L46
Aviles A., Bravetti A., Capozziello S., Luongo O., 2014, Phys. Rev. D, 90,
    043531
Avni Y., Tananbaum H., 1982, ApJ, 262, L17
Bernal J. L., Verde L., Riess A. G., 2016, J. Cosmology Astropart. Phys.,
    2016, 019
Birrer S., et al., 2019, MNRAS, 484, 4726
Birrer S., et al., 2020, A&A, 643, A165
Blandford R. D., Narayan R., 1992, ARA&A, 30, 311
Bloom J. S., Frail D. A., Sari R., 2001, AJ, 121, 2879
Bonvin V., et al., 2017, MNRAS, 465, 4914
Butler N. R., Kocevski D., Bloom J. S., 2009, ApJ, 694, 76
Capozziello S., De Laurentis M., Luongo O., Ruggeri A., 2013, Galaxies, 1,
    216
Capozziello S., D'Agostino R., Luongo O., 2018, MNRAS, 476, 3924
Capozziello S., D'Agostino R., Luongo O., 2019, International Journal of
    Modern Physics D. 28, 1930016
Cattoën C., Visser M., 2008, Phys. Rev. D, 78, 063501
Chen G. C. F., et al., 2019, MNRAS, 490, 1743
Collett T. E., Auger M. W., 2014, MNRAS, 443, 969
Collett T., Montanari F., Räsänen S., 2019, Phys. Rev. Lett., 123, 231101
D'Amico G., Senatore L., Zhang P., Zheng H., 2021, J. Cosmology Astropart.
    Phys., 2021, 072
Dai Z. G., Liang E. W., Xu D., 2004, ApJ, 612, L101
Demianski M., Piedipalumbo E., Sawant D., Amati L., 2017, A&A, 598,
    A112
Demianski M., Piedipalumbo E., Sawant D., Amati L., 2021, MNRAS,
Denzel P., Coles J. P., Saha P., Williams L. L. R., 2021, MNRAS, 501, 784
Di Valentino E., Melchiorri A., Silk J., 2020, Nature Astronomy, 4, 196
Di Valentino E., et al., 2021, Classical and Quantum Gravity, 38, 153001
Feroci M., et al., 2012, Experimental Astronomy, 34, 415
Freedman W. L., et al., 2019, ApJ, 882, 34
Gavazzi R., Treu T., Koopmans L. V. E., Bolton A. S., Moustakas L. A.,
    Burles S., Marshall P. J., 2008, ApJ, 677, 1046
Gehrels N., et al., 2004, ApJ, 611, 1005
Ghirlanda G., Ghisellini G., Firmani C., 2006, New Journal of Physics, 8, 123
Goldstein A., Connaughton V., Briggs M. S., Burns E., 2016, ApJ, 818, 18
Götz D., et al., 2009, in Meegan C., Kouveliotou C., Gehrels N., eds,
    American Institute of Physics Conference Series Vol. 1133, Gamma-
```

ray Burst: Sixth Huntsville Symposium. pp 25–30 (arXiv:0906.4195),

```
Jee I., Suyu S. H., Komatsu E., Fassnacht C. D., Hilbert S., Koopmans L.
    V. E., 2019, Science, 365, 1134
Kessler R., Scolnic D., 2017, ApJ, 836, 56
Khadka N., Ratra B., 2021, MNRAS,
Khadka N., Luongo O., Muccino M., Ratra B., 2021, arXiv e-prints, p.
    arXiv:2105.12692
Knox L., Millea M., 2020, Phys. Rev. D, 101, 043533
Li E.-K., Du M., Xu L., 2020, MNRAS, 491, 4960
Liang E., Zhang B., 2005, ApJ, 633, 611
Liao K., 2019, Phys. Rev. D, 99, 083514
Lusso E., Risaliti G., 2017, A&A, 602, A79
Lusso E., et al., 2020, A&A, 642, A150
Marra V., Amendola L., Sawicki I., Valkenburg W., 2013, Phys. Rev. Lett.,
    110, 241305
Marriner J., et al., 2011, ApJ, 740, 72
Meegan C., et al., 2009, ApJ, 702, 791
Nava L., et al., 2012, MNRAS, 421, 1256
Oguri M., 2019, Reports on Progress in Physics, 82, 126901
Oguri M., Marshall P. J., 2010, MNRAS, 405, 2579
Planck Collaboration et al., 2020, A&A, 641, A6
Qi J.-Z., Zhao J.-W., Cao S., Biesiada M., Liu Y., 2020, arXiv e-prints, p.
    arXiv:2011.00713
Räsänen S., Bolejko K., Finoguenov A., 2015, Phys. Rev. Lett., 115, 101301
Refsdal S., 1964, MNRAS, 128, 307
Riess A. G., 2019, Nature Reviews Physics, 2, 10
Riess A. G., et al., 2011, ApJ, 730, 119
Riess A. G., et al., 2016, ApJ, 826, 56
Riess A. G., Casertano S., Yuan W., Macri L. M., Scolnic D., 2019, ApJ, 876,
Riess A. G., Casertano S., Yuan W., Bowers J. B., Macri L., Zinn J. C., Scolnic
    D., 2021, ApJ, 908, L6
Risaliti G., Lusso E., 2019, Nature Astronomy, 3, 272
Rusu C. E., et al., 2020, MNRAS, 498, 1440
Schneider P., Ehlers J., Falco E. E., 1992, Gravitational Lenses,
    doi:10.1007/978-3-662-03758-4.
Scolnic D. M., et al., 2018, ApJ, 859, 101
Shafieloo A., Sahni V., Starobinsky A. A., 2012, Phys. Rev. D, 86, 103527
Shajib A. J., et al., 2019, MNRAS, 483, 5649
Shajib A. J., et al., 2020, MNRAS, 494, 6072
Speagle J. S., 2020, MNRAS, 493, 3132
Suyu S. H., Marshall P. J., Auger M. W., Hilbert S., Blandford R. D., Koop-
    mans L. V. E., Fassnacht C. D., Treu T., 2010, ApJ, 711, 201
Suyu S. H., et al., 2014, ApJ, 788, L35
Suyu S. H., Chang T.-C., Courbin F., Okumura T., 2018, Space Sci. Rev.,
    214, 91
Taubenberger S., et al., 2019, A&A, 628, L7
Treu T., Marshall P. J., 2016, A&ARv, 24, 11
Tripp R., 1998, A&A, 331, 815
Trotta R., 2017, arXiv e-prints, p. arXiv:1701.01467
Velten H., Gomes S., 2020, Phys. Rev. D, 101, 043502
Verde L., Protopapas P., Jimenez R., 2013, Physics of the Dark Universe, 2,
Verde L., Treu T., Riess A. G., 2019, Nature Astronomy, 3, 891
Visser M., 2004, Classical and Quantum Gravity, 21, 2603
Wang F. Y., Dai Z. G., Liang E. W., 2015, New Astron. Rev., 67, 1
Wei J.-J., Melia F., 2020, ApJ, 897, 127
Wong K. C., et al., 2017, MNRAS, 465, 4895
Wong K. C., et al., 2020, MNRAS, 498, 1420
Yang T., Banerjee A., Ó Colgáin E., 2020, Phys. Rev. D, 102, 123532
Zhang B., 2018, The
                                 Physics of Gamma-Ray
    doi:10.1017/9781139226530.
```

Jee I., Komatsu E., Suyu S. H., Huterer D., 2016, J. Cosmology Astropart.

Phys., 2016, 031

doi:10.1063/1.3155898

Ivezić Ž., et al., 2019, ApJ, 873, 111

Gruber C., Luongo O., 2014, Phys. Rev. D, 89, 103506

APPENDIX A: APPENDIX

In this appendix, we present the formulas for the parametrizations of the cosmic distances used in the general cosmography.

The leading-order cosmographic parameters are defined as the scale factor deviations in terms of cosmic time:

$$H(t) \equiv \frac{1}{a} \frac{da}{dt}, q(t) \equiv -\frac{1}{aH^2} \frac{d^2a}{dt^2}, j(t) \equiv \frac{1}{aH^3} \frac{d^3a}{dt^3}, s(t) \equiv \frac{1}{aH^4} \frac{d^4a}{dt^4}, \tag{A1}$$

which are respectively referred to the Hubble, deceleration, jerk, and snap parameters, etc. With these definitions, we investigate the cosmic expansion with expanding the scale factor into a Taylor series around the present time t_0 (z = 0),

$$\frac{a(t)}{a(t_0)} = 1 + H_0(t - t_0) - \frac{1}{2}q_0H_0^2(t - t_0)^2 + \frac{1}{6}j_0H_0^3(t - t_0)^3 + \frac{1}{24}s_0H_0^4(t - t_0)^4 + \dots].$$
(A2)

Using the FLRW geometry and the definition of redshift z = 1/a(t) - 1 with simply assuming $a(t_0) = 1$, we then obtain the dimensionless co-moving distance as a function of redshift with the fourth-order cosmographic parameters.

$$d(z) = z - \frac{1}{2}(1+q_0)z^2 + \frac{1}{6}(2+4q_0+3q_0^2-j0+\Omega_{K,0})z^3$$
$$-\frac{1}{24}[6+18q_0-27q_0^2-15q_0^3-(9+10q_0)j_0 \qquad (A3)$$
$$-s_0 + (6+6q_0)\Omega_{K,0}]z^4 + O(z^5).$$

To mitigate the convergence problem that the cosmographic expansion encounters at higher redshift (e.g., z > 1), it is useful to recast the d(z) in the form of the *y-redshift*, y = z/(1+z). In this manner, the distance in $z \in (0, \infty)$ is mapped into $y \in (0, 1)$, whereby the cosmographic expansions would be well behaved in the redshift range from the local universe to the "Big Bang". Thus, with the change of variable $z :\rightarrow y$, the dimensionless co-moving distance becomes

$$d(y) = y + \frac{1}{2}(1 - q_0)y^2 + \frac{1}{6}(2 - 2q_0 + 3q_0^3 - j_0 + \Omega_{K,0})y^3 + \frac{1}{24}[6 - 6q_0 + 9q_0^2 - 15q_0^3 - (3 - 10q_0)j_0 + s_0 + (6 - 6q_0)\Omega_{K,0}]y^4 + O(y^5).$$
(A4)

With the relation of $d(z) = H_0 d_L(z)/c(1+z)$, the luminosity distance in the FLRW universe is given by

$$\begin{split} d_{\rm L}(z) &= \frac{c}{H_0} \{z + \frac{1}{2} (1 - q_0) z^2 - \frac{1}{6} (1 - q_0 - 3q_0^3 + j0 - \Omega_{K,0}) z^3 \\ &\quad + \frac{1}{24} [2 - 2q_0 - 15q_0^2 - 15q_0^3 + (5 + 10q_0) j_0 \\ &\quad + s_0 - (2 + 6q_0) \Omega_{K,0}] z^4 + O(z^5) \}. \end{split} \tag{A5}$$

In terms of the y-redshift, $d_{\rm L}(z)$ is converted to

$$\begin{split} d_{\rm L}(y) &= \frac{c}{H_0} \{ y + \frac{1}{2} (3 - q_0) y^2 + \frac{1}{6} (11 - 5q_0 + 3q_0^2 - j0 + \Omega_{K,0}) y^3 \\ &+ \frac{1}{24} [50 - 26q_0 + 21q_0^2 - 15q_0^3 - (7 - 10q_0) j_0 \\ &+ s_0 + (10 - 6q_0) \Omega_{K,0}] y^4 + O(y^5) \}. \end{split} \tag{A6}$$

The distance modulus $\mu(z) = 5 \log[d_L(z)/\text{Mpc}] + 25$ can be obtained from the "logarithmic Hubble relation": $\ln(d_L(y)/\text{Mpc})/y = \ln 10/5[\mu(y) - 25] - \ln y$, which gives

$$\mu(y) = 25 + \frac{5}{\ln 10} \{ \ln(c/H_0) + \ln y + \frac{1}{2} (3 - q_0)y + \frac{1}{24} [17 - 2q_0] + 9q_0^2 - 4(j_0 - \Omega_{K,0}) \} y^2 + \frac{1}{24} [11 - q_0 + 2q_0^2 - 10q_0^3 - (1 - 8q_0)j_0] + s_0 + (16 - 4q_0)\Omega_{K,0} \} y^3 + O(y^4) \}.$$
(A7)